Variability in the Concentration of Lithium in the Indo-Pacific Ocean

Zvi Steiner[1] , William M. Landing[2] , Madeleine S. Bohlin[3,4] , Mervyn Greaves[4] , Satya Prakash[5], P. N. Vinayachandran[6] , and Eric P. Achterberg[1]

[1]GEOMAR Helmholtz Centre for Ocean Research Kiel, Kiel, Germany, [2]Department of Earth, Ocean & Atmospheric Science, Florida State University, Tallahassee, FL, USA, [3]Department of Earth Sciences, Uppsala University, Uppsala, Sweden, [4]Department of Earth Sciences, University of Cambridge, Cambridge, UK, [5]Indian National Centre for Ocean Information Services, Hyderabad, India, [6]Centre for Atmospheric and Oceanic Sciences, Indian Institute of Science, Bangalore, India

Abstract Lithium has limited biological activity and can readily replace aluminium, magnesium and iron ions in aluminosilicates, making it a proxy for the inorganic silicate cycle and its potential link to the carbon cycle. Data from the North Pacific Ocean, tropical Indian Ocean, Southern Ocean and Red Sea suggest that salinity normalized dissolved lithium concentrations vary by up to 2%–3% in the Indo-Pacific Ocean. The highest lithium concentrations were measured in surface waters of remote North Pacific and Indian Ocean stations that receive relatively high fluxes of dust. The lowest dissolved lithium concentrations were measured just below the surface mixed layer of the stations with highest surface water concentrations, consistent with removal into freshly forming aluminium rich phases and manganese oxides. In the North Pacific, water from depths >2,000 m is slightly depleted in lithium compared to the initial composition of Antarctic Bottom Water, likely due to uptake of lithium by authigenically forming aluminosilicates. The results of this study suggest that the residence time of lithium in the ocean may be significantly shorter than calculated from riverine and hydrothermal fluxes.

1. Introduction

Scientific interest in lithium has been rapidly growing in recent years owing to its wide range of industrial applications, notably its use in the manufacture of lithium-ion batteries, ceramics and glass (Swain, 2017). In environmental science, lithium concentrations, and lithium isotope ratios, have been shown to be useful tools to quantify rates of silicate weathering and secondary mineral precipitation in river systems (Bohlin & Bickle, 2019; Huh et al., 1998; Pogge von Strandmann et al., 2012; Tomascak et al., 2016), and chemical reactions occurring in hydrothermal systems (Edmond et al., 1979; Seyfried et al., 1984). River and hydrothermal inputs are the main sources of lithium to the ocean, although there are smaller sources from atmospheric deposition and ground-water discharge (Stoffyn-Egli & Mackenzie, 1984). The sensitivity of seawater lithium isotope composition to continental weathering and hydrothermal activity makes it a powerful tool for the reconstruction of past chemical weathering and the related effect on global climate (Hathorne & James, 2006; Li & West, 2014; Misra & Froelich, 2012).

The residence time of lithium in the ocean, calculated from riverine and hydrothermal fluxes, is 1.5–1.8 million years (Huh et al., 1998; Lecuyer, 2016), much longer than the mixing time of the ocean (~1,600 years), leading to the conclusion that lithium is well mixed and that seawater lithium concentrations and isotope ratios at any given time period are constant (Chan & Edmond, 1988; Hathorne & James, 2006; Li & West, 2014; Misra & Froelich, 2012). However, the few studies that analyzed lithium concentrations in the subtropical gyre of the North Atlantic Ocean suggested that Li/Cl ratios in the upper 1,200–1,400 m are ~2% higher than Li/Cl ratios of the deep waters (Angino & Billings, 1966; Fabricand et al., 1966; Stoffyn-Egli & Mackenzie, 1984). Lithium concentrations are also elevated in some coastal regions (Fujinaga et al., 1980). Lithium appears to mix conservatively between freshwater and seawater (Brunskill et al., 2003; Stoffyn-Egli, 1982), though evidence for removal of lithium in estuaries has been reported (Pogge von Strandmann et al., 2008). On the other hand, sporadic samples from the subpolar North Atlantic, Southern and Pacific Oceans did not show systemic variability in the concentration of lithium (Chow & Goldberg, 1962; Riley & Tongudai, 1964). Initially published δ⁷Li values for

seawater varied over 5‰, however later work has suggested that much of this range is due to analytical issues, and the global ocean has uniform δ^7Li = 30.8 ± 0.4‰ (Carignan et al., 2004; Rosner et al., 2007).

The observation that Li/Cl in the North Atlantic Ocean is not constant, and that the residence time of lithium in the ocean is much shorter than the residence time of the heavier alkali metals sodium and potassium (1.5–1.8 Ma for lithium compared to about 40 Ma for sodium and 8 Ma for potassium; Lecuyer, 2016), may hint at an active short-term oceanic lithium cycle. The ionic radius of Li$^+$ is similar to Mg^{2+}, Fe^{2+}, and Al^{3+}, and lithium can often substitute for magnesium in the octahedral sites of clays (Hindshaw et al., 2019; Jiang et al., 2007). Lithium rarely participates in biological cycles (Lemarchand et al., 2010; Schmitt et al., 2012), though it is found in varying concentrations in the tissues of marine organisms (Thibon et al., 2021). The partition coefficient of lithium from seawater in calcium carbonate minerals is 0.01–0.0005 (Dellinger et al., 2018; Langer et al., 2020), and the lithium content of biogenic opal is also low (Martin et al., 1991). The fact that lithium does not partition strongly into biominerals suggests that lithium could act as a reliable proxy for water-solid interactions such as dissolution and precipitation of aluminosilicates in the ocean, with the added note that as a stable dissolved major element with long residence time, lithium is less influenced than other elements by redox conditions and pH.

In many cases, the distribution of trace elements in seawater helps elucidate their sources and sinks and their potential cycling in the water column but provides less information regarding processes that determine their residence time in the ocean. This gap is particularly important when trying to understand the rates and fate of atmospheric deposition of trace elements, which is a major source of macro and micro-nutrients to remote ocean regions (Martin, 1990). Studies of atmospheric deposition often use aluminium, thorium, beryllium or iron to quantify deposition rates. However, since iron is an essential micronutrient, and aluminium, beryllium, iron and thorium have very short residence times in the ocean, these calculations are highly susceptible to model assumptions (Baker et al., 2016; Menzel Barraqueta et al., 2019). Data on lithium concentrations may provide an additional constraint on atmospheric deposition to the ocean and are particularly useful in relation to the aluminium cycle since both lithium and aluminium are intricately related to the inorganic silicate cycle. An important difference between the aluminium and lithium cycles is that aluminium is also strongly involved in the biogenic silica cycle (Menzel Barraqueta et al., 2018; Moran & Moore, 1988). As analytical techniques have progressed, it is appropriate to revisit the question of the distribution of lithium within the global oceans, given that we can now analyze lithium concentrations to far higher precision and with much higher throughput than previously possible. In this paper we explore the variability in lithium concentration in the global ocean using lithium concentration measurements from a range of ocean transects.

2. Materials and Methods

2.1. Seawater Sampling and Study Area

2.1.1. North Pacific

North Pacific water samples were collected during cruise CDisK-IV from Hawaii to Alaska in 01–30 August 2017 on board RV Kilo Moana, roughly along 150°W (Figure 1). Full depth profiles were obtained at five stations, from Station ALOHA in the south to Ocean Station Papa in the north. Additional surface water samples were collected every 1–1.5° from the ship's underway water system. The samples were filtered using 0.22 μm Millipore polyether sulfone (PES) syringe filters into acid washed low density polyethylene (LDPE) bottles and acidified with distilled HNO$_3$ to final HNO$_3$ concentration of 0.02 N.

The North Pacific transect ran from the center of the subtropical gyre into the far more productive subpolar gyre. The transition zone between the gyres shifts seasonally between 32°N and 42°N (Ayers & Lozier, 2010; Polovina et al., 2017; Roden, 1991). At the time of CDisK-IV, the transition zone chlorophyll front was located at 37°N (Hou et al., 2019). Dust blown from Asia is a major source of sediment and nutrients to the study area, particularly in the region between about 30 and 45°N (Buck et al., 2013; Ginoux et al., 2001; Jickells et al., 2005; Zender et al., 2003). The North Pacific Current is the main surface ocean current crossed in this transect. The North Pacific Current originates from the Kuroshio extension, and is located around 42°N along 150°W. Closer to North America, the North Pacific Current bifurcates and its extensions form the Alaska and California currents (Cummins & Freeland, 2007). Pacific deep-water forms from mixing and sinking of water masses in the Southern Ocean. Deep-water flow rates in the northeast Pacific are often too low for reliable direct measurements,
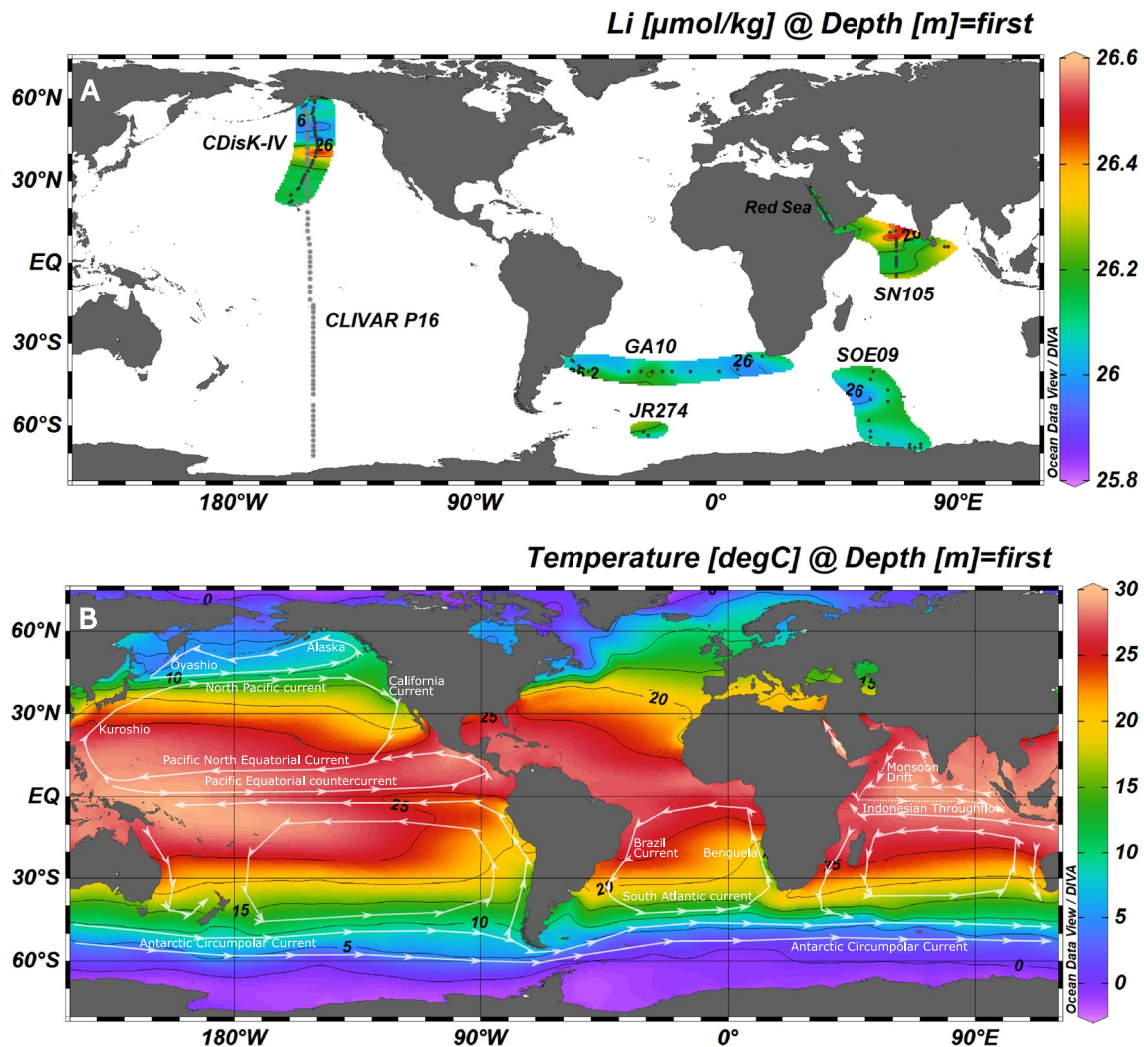
Figure 1. (a) Sampling locations and surface water concentration of dissolved lithium, normalized to TEOS-10 absolute salinity of 35 g kg^{-1} (IOC et al., 2010; McDougall & Barker, 2011). (b) Annual average surface water temperature and major ocean currents in the studied regions. Direction arrows for North Indian Ocean currents are drawn for the winter monsoon; flow directions reverse seasonally. Temperature data are from the World Ocean Atlas 2013 annual data of the years 1955–2012 (https://odv.awi.de/data/ocean/world-ocean-atlas-2013/). Maps prepared using ODV 5.3.0 (Schlitzer, 2020).

however, ^{14}C ages suggest it takes about 1,000 years for Antarctic Bottom Water (AABW) and Lower Circumpolar Deep Water (LCDW) to reach the study region (Matsumoto, 2007).

2.1.2. Tropical Indian Ocean

Tropical Indian Ocean samples were obtained on cruise SN105 on board ORV Sagar Nidhi along 67°E from 12°N to 5°S in 07 to 16 December 2015. The samples were filtered using 0.22 μm Millipore PVDF syringe filters into polypropylene tubes (PP) and kept refrigerated until analysis. The concentrations of strontium and Sr/Ca ratios were previously reported for the same samples (Steiner et al., 2020). Strontium concentrations along the SN105 transect abruptly increase by ~2% at 50–70 m, implying poor mixing between the surface and intermediate waters. The physical oceanography and biogeochemistry of the studied region are influenced by seasonal reversals in the monsoon winds (Hood et al., 2017). Cruise SN105 took place during the northeast monsoon, when winds blow to the study region from the Indian subcontinent and primary productivity is low. The intermediate water column of the region is characterized by three layers of regionally produced water masses. Immediately below the surface mixed layer are high salinity Arabian Sea Surface Waters, Persian Gulf waters centered at ~250 m and the Red Sea water mass centered at 750–900 m (Rochford, 1964; Shenoi et al., 1993).

Red Sea surface water samples, and a few additional surface water samples from the Indian Ocean, were collected with a bucket lowered from the deck of a container ship during 27 December 2015 to 3 January 2016 and 23–31 March 2018. Full description of sample retrieval and handling was provided in Steiner et al. (2018).

2.1.3. Southern Ocean

Samples were retrieved from the Indian Ocean sector of the Southern Ocean on cruise SOE09 on board S. A. Agulhas I in 12 January to 21 February 2017. The samples were stored unfiltered in PP tubes and kept refrigerated until analysis. Additional Southern Ocean samples were collected during the UK ocean acidification cruise JR274 in the Atlantic sector between 9 January and 12 February 2013 on board RRS James Clark Ross. The JR274 samples were analyzed to test the coherence of the Southern Ocean data, and whether the different sampling and preservation strategies of the different cruises affect the results. The JR274 samples were sampled with trace metal clean samplers, filtered through cartridge filters (0.2 mm Sartobran P300, Sartorius), and stored in 125 mL LDPE bottles (Nalgene). The samples were acidified on-board with ultra-clean HNO_3 to pH = 1.7 (Schlosser et al., 2018). The Southern Ocean receives far less dust than most ocean regions. As a result, primary productivity in the Southern Ocean is normally iron limited (Martin, 1990). Surface water lithium concentrations are also reported for the GEOTRACES GA10 transect, which was covered in two cruises from South Africa to South America, mostly along 40°S; cruise D357 on board SSR Discovery in 18 October to 22 November 2010, and cruise JC068 on board RRS James Cook in 24 December 2011 to 27 January 2011. The GA10 transect roughly followed the subtropical front. The dominant surface water masses change in an east to west direction starting from the Agulhas Current near the African coast, followed by Sub-Antarctic Surface Water, Sub-Tropical Surface Water, and the Brazil Current near the South American coast (Wyatt et al., 2014).

2.2. Analyses of Lithium Concentrations in Seawater

Lithium concentrations were analyzed using inductively coupled plasma optical emission spectroscopy (ICP-OES) using a sample-standard bracketing method (de Villiers et al., 2002; Schrag, 1999) modified for analyses of major element concentrations in seawater (Steiner et al., 2018, 2020). The ICP-OES reads the intensity of light emitted by all elements simultaneously, which is a major advantage over other plasma instruments since analysis of element ratios eliminates uncertainties related to plasma and pump instability. Another advantage of simultaneous analyses is that by analyzing the concentration ratio of the element of interest to sodium, the data are salinity-normalized. This eliminates variations related to changes in salinity, evaporation from vials and small dilution errors. Element-to-sodium ratios are then converted to concentrations by multiplying them with sodium concentrations at TEOS-10 absolute salinity (S_A) of 35 g kg^{-1}. Salinity-normalized lithium concentrations that have been thus corrected will henceforth be referred to as lithium concentrations. This calculation assumes that sodium-to-salinity ratios of seawater are constant everywhere in the ocean, an assumption embedded in the modern definition of salinity (Millero et al., 2008). The molarity of sodium in seawater is 18,000 times the molarity of lithium, hence reactions that affect sodium and lithium in similar absolute terms are analytically undetectable for sodium.

Lithium and sodium concentrations of most samples were measured at the University of Cambridge using an Agilent Technologies 5100 ICP-OES based on the Li670.783 and Na568.821 spectral lines, after dilution of the samples to salinity of 0.42 g kg^{-1} (~130 μg g^{-1} Na) with 0.1 N HNO_3. Lithium and sodium concentration for samples from cruises JR274, D357 and RJ068 were measured using a Varian 720 ICP-OES at GEOMAR Helmholtz Center for Ocean Research Kiel, using the same set of standards, based on the Li670.783 and Na330.237 spectral lines. A calibration curve was obtained using different dilutions of an IAPSO standard seawater from batch P157. An IAPSO sample matched to the salinity of the diluted samples served as a consistency standard for the sample-standard bracketing. Each measurement consisted of 5–6 consecutive scans for 5 s (Cambridge) or 10 s (GEOMAR), and the samples were analyzed in duplicate later in the analytical session, and often analyzed again on a different day. Lithium concentrations in the IAPSO standard were determined at GEOMAR by standard additions of LiCl (99.999%, Roth). According to this calibration, the concentration of lithium in the IAPSO standard is 26.16 ± 0.45 μmol kg^{-1} (normalized to TEOS-10 absolute salinity of 35 g kg^{-1}). The consistency standard was analyzed as an additional sample in the standard-standard bracketing in each of the ICP-OES sessions; the long term 2σ SD of the consistency standard is 0.24% (0.06 μmol kg^{-1} Li) (Figure 2).
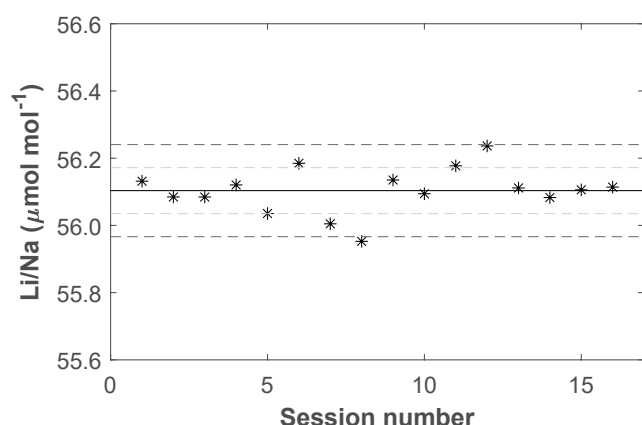
Figure 2. Li/Na of the IAPSO P157 consistency standard analyzed as additional samples in the different ICP-OES sessions. The solid line represents the average of the IAPSO standard runs, the dashed lines represent ±1σ standard deviation (light gray, 0.12%) and ±2σ standard deviation (dark gray, 0.24%). The figure includes analytic sessions from both the University of Cambridge (sessions 1–9) and GEOMAR (sessions 10–16).

2.3. Lithium Isotopic Composition

2.3.1. Li Purification

All acids used for sample preparation and lithium isotope analysis were double distilled in a Teflon sub-boiling still and diluted to the required concentrations using 18.2 MΩ · cm MilliQ water. Purification of Li from other sample matrix elements and subsequent isotope analysis followed the procedure of Bohlin et al. (2018). Samples containing approximately 2 ng of Li were evaporated on a hot plate and refluxed in concentrated HNO_3 for 24 hr at 110°C to break down organic matter present in the sample matrix. The samples were then dried down and dissolved in 200 μL of 0.7 N HCl ready for column chromatography.

High aspect ratio columns (3 mL volume—250 mm height and 4 mm inner diameter) were filled with AGMP-50 macro-porous cation exchange resin. The resin was thoroughly cleaned with 10 N HCl and MilliQ water and then "backwashed" in MilliQ water using a handheld pump. During backwashing the resin is suspended and let to resettle by gravity, providing a homogenous resin bed. After conditioning the resin with 0.7 N HCl, each sample was loaded onto the columns in duplicate and treated as separate samples during processing and subsequent analyses. After loading, the columns were washed with 9 ml 0.7 N HCl. Li was then eluted in 13 mL of 0.7 N HCl and collected in Teflon vials. Fractions (1 mL) were collected before and after the Li was eluted and kept for potential Li concentration measurements in case of Li peak migration. These measurements are only performed if the δ⁷Li value of the external standards (which are processed together with the samples), deviated from the certified or established value, and in the end were not necessary in this study. The samples were evaporated on a hot plate, refluxed in concentrated nitric acid at 110°C for 24 hr, dried down again and dissolved in 1 ml 0.32 N HNO_3 for isotope analysis.

2.3.2. Li Isotope Analysis

The isotopic composition of Li was measured via multi-collector inductively coupled plasma mass spectrometry (MC-ICP-MS) on the Thermo Scientific Neptune PLUS at the University of Cambridge. A quartz ApexIR sample introduction system was used, containing a 140°C spray chamber and 2°C Peltier cooling coil. A 100 μL min⁻¹ Savillex C-spray self-aspirating nebulizer, Ni-Jet sampler and Ni-X skimmer cones were used, generating 0.4 V on ⁷Li for a 0.5 ng ml⁻¹ solution. Both ⁶Li and ⁷Li were measured using 10^{13} Ω amplifiers, in the L4 and H4 cups respectively. Samples were analyzed using the sample-standard bracketing method with NIST 8545 L-SVEC as bracketing standard. The concentrations of samples and standards were matched to within 10% of each other. Blanks were measured before and after each sample and standard and had a maximum intensity of 3 mV, or 0.75% of the sample intensity. Samples were measured as a block containing 25 cycles with 8.4 s integration time. Results are reported in ‰ using delta notation:

$$\delta^7\text{Li} = \left(\frac{(^7\text{Li}/^6\text{Li})_{\text{sample}}}{\frac{(^7\text{Li}/^6\text{Li})_{\text{L-SVEC1}} + (^7\text{Li}/^6\text{Li})_{\text{L-SVEC2}}}{2}} - 1 \right) \times 1,000 \qquad (1)$$

where the ⁷Li/⁶Li ratio of the sample is reported relative to the average ratio of the L-SVEC measured immediately before and after the sample. The results in table 1 are given as the average of the two procedural replicates. The long-term external reproducibility of the method is 0.4‰, based on past work (Bohlin et al., 2018). The secondary standard Li7-N yielded a value of 30.11 ± 0.12‰ (n = 2) in this study, in agreement with previous studies (Bohlin et al., 2018; Carignan et al., 2007). North Atlantic seawater from 1,000 m in the center of the subtropical gyre was used as a full procedural standard and yielded a value of 31.0 ± 0.3‰ (n = 5) (Table 1).

Table 1
δ^7Li Values of Seawater Samples From This Study

	Latitude	Longitude	Depth (m)	$[Li]_{normalised}$ ($\mu mol\ kg^{-1}$)	2σ ($\mu mol\ kg^{-1}$)	δ^7Li (‰)	2σ (‰)
L-SVEC						−0.18	
North Atlantic			1,000			31.00	0.29
Pacific	41.72°N	148.30°W	3	26.37	0.12	30.78	0.12
Pacific	41.72°N	148.30°W	3,804	25.97	0.02	30.89	0.24
Indian	9.00°N	66.98°E	3	26.65	0.14	30.88	0.31
Red Sea	13.72°N	42.58°E	0	26.17	0.001	30.94	0.06

Note. The average values of two procedural replicates are given with their 2σ standard deviation (five procedural replicates for the North Atlantic in-house standard). Long-term external 2σ standard deviations are 0.4‰ for analyses of δ^7Li values and 0.06 $\mu mol\ kg^{-1}$ for lithium concentrations. δ^7Li value of the LSVEC standard is defined as 0‰ and reported for LSVEC samples run as samples bracketed by LSVEC standards.

2.4. Aerosol Samples

Daily aerosol samples were collected from the Pacific Ocean during CLIVAR-CO$_2$ Repeat Hydrography Section P16. The P16 section follows 150°–152°W and was divided into two legs, a southern leg from 17°S to 71°S in January to February 2005, and a northern leg from 16°S to 56°N in February to March 2006. Additional aerosol data from CLIVAR-CO$_2$ section P2 from Japan to San Diego, along 30°N, visited in June to August 2004, are provided in Supporting Information S1 and Table S2 in Supporting Information S1. Description of the sampling and analytical methods, as well as iron, aluminium and manganese concentration data and flux calculations are provided in Buck et al. (2013). The P16 North Pacific aerosol data were collected in a different season than the dissolved lithium data.

The aerosol-collecting system obtained samples for periods of 24 hr and was automatically set to power off the pumps when the direction of the wind was outside ±60° of the bow, or the wind speed was <0.5 m/s. The filter head was fitted with an unwashed 0.45 μm polycarbonate filter of 47 mm diameter.

The polycarbonate filters from the aerosol samplers were analyzed for chlorine concentrations at the NOAA/PMEL laboratory using energy dispersive X-ray fluorescence (EDXRF). For total aerosol lithium concentrations, the individual filters were submerged in a HF:HNO$_3$:HCl mixture and heated to 180°C (30 min ramp time, 30 min hold time) in sealed Teflon digestion vessels. The resulting solution was rinsed from the vessel using deionized water and transferred to acid-washed 60 mL LDPE wide-mouth bottles. The solution was dried on a hot plate and then rehydrated with 50 mL of deionized water, acidified to 0.024 M Q-HNO$_3$, and analyzed with HR-ICP-MS at the National High Magnetic Field Laboratory in Tallahassee, Florida using multielement standards and 1 ppb Sc as an internal standard. To eliminate the contribution of lithium from sea spray we define excess total aerosol lithium (Li_{xs-tot}) as:

$$Li_{xs-tot} = [Li]_{measured} - [Cl]_{measured} \cdot \left(\frac{[Li]}{[Cl]} \right)_{seawater} \tag{2}$$

$[Li]_{measured}$ and $[Cl]_{measured}$ refer to the total concentrations measured on the filters. $([Li]/[Cl])_{seawater}$ is the global average ratio, 0.0478 mmol mol^{-1}.

The deposition flux is calculated by applying bulk (wet + dry) deposition velocity to the concentration (Figure S1 in Supporting Information S1). We calculate the bulk deposition velocity based on the rain rate in different latitudes along the P16 transect following Kadko et al. (2020):

$$\text{Bulk deposition velocity } \left(m\,day^{-1} \right) = 365,000 \pm 35,000 \times \text{Rain Rate } \left(m\,day^{-1} \right) + 1,040 \pm 136 \left(m\,day^{-1} \right) \tag{3}$$

3. Results

In the North Pacific, salinity-normalized lithium concentrations are higher in the top 2,000 m of the water column (26.11 ± 0.10 μmol kg^{-1}, 1σ SD) relative to samples from >2,000 m (26.00 ± 0.07 μmol kg^{-1}) (Figure 3a). The average difference in lithium concentrations between the deep and intermediate North Pacific waters is only slightly larger than the 2σ SD of the analytical method (0.06 μmol kg^{-1}) but were consistent throughout the transect. A two-sided *t*-test rejects the hypothesis that the mean lithium concentrations of the two subsets is equal ($p < 0.001$), the 95% confidence interval for the mean difference between samples >2,000 and <2,000 m is 0.08–0.14 μmol kg^{-1}. Lithium concentrations are constant across the Indian sector of the Southern Ocean transect SOE09 (Figure 3b; 26.12 ± 0.08 μmol kg^{-1}), and similar to the two JR274 Weddel Sea stations analyzed (26.09 ± 0.11 μmol kg^{-1}, $p = 0.09$). The mean lithium concentration of the Southern Ocean samples (SOE09 and JR274 data combined) is similar to <2,000 m North Pacific samples ($p = 0.38$) and higher than the mean deep North Pacific lithium concentration by 0.09–0.14 μmol kg^{-1} (95% confidence interval, $p < 0.001$). Lithium concentration data from the tropical Indian Ocean are restricted to the top 2,000 m (Figure 3c). The average lithium concentration in the tropical Indian Ocean section (26.18 ± 0.11 μmol kg^{-1}) is slightly higher than lithium concentrations in the same depth range in the North Pacific and Southern Oceans. A *t*-test rejects the hypothesis that the mean lithium concentrations of the tropical Indian and North Pacific samples from the top 2,000 m are equal ($p < 0.001$), the 95% confidence interval for the mean difference between the subsets is 0.05–0.10 μmol kg^{-1}. Average Red Sea surface water concentration (Table S1 in Supporting Information S1; 26.18 ± 0.09 μmol kg^{-1}) is similar to the mean Indian Ocean concentration.

There is non-random variability in the surface water concentrations of lithium of the North Pacific and tropical Indian Ocean transects (Figures 4 and 5). In the Hawaii-to-Alaska transect, surface water lithium concentrations are 26.14 ± 0.02 (1σ SD) μmol kg^{-1} between 22°N and 31°N. Surface water lithium concentrations are higher in the transition zone between the subtropical and subpolar gyres and reach a peak concentration of 26.51 μmol kg^{-1} at 40.4°N. The location of peak surface water lithium concentrations is approximately at the northern end of the transition zone between the subtropical and subpolar gyres of the North Pacific. Lithium concentrations in the transition zone are only elevated in the surface mixed layer (Figure 5a). The lowest lithium concentrations of the entire profile are found between 30 and 100 m depth, at the station with the highest surface water lithium concentrations (Figure 5a). In the North Pacific subpolar gyre, surface water lithium concentrations decrease to 26.02 ± 0.06 μmol kg^{-1} between 45°N and 59°N, similar to the deep-water lithium concentrations from this transect (Figure 3a). In the tropical Indian Ocean section, surface water lithium concentrations are 1.5%–2% higher at 9–12°N compared to the rest of the section (Figure 4b).

We analyzed δ^{7}Li values in selected samples with particularly high or low lithium concentrations to test the hypothesis that δ^{7}Li values of seawater vary where maximum variations in lithium concentrations are observed (Table 1). The results support previous assertions that all variability in δ^{7}Li values of the global ocean is within the limitations of the analytical methods (Carignan et al., 2004; Rosner et al., 2007).

There is qualitative agreement between the spatial patterns in surface water lithium concentrations in the North Pacific and aerosol total excess lithium (Li$_{xs\_tot}$; Equation 2; Figure 6). Lithium excess in the North Pacific are higher in the western than eastern part of the basin, suggesting Asian source of the exess lithium (Figure S2 in Supporting Information S1).

4. Discussion

In both the North Pacific and tropical Indian Ocean transects, the lowest lithium concentrations were measured within the top 100 m of the water column at the same locations where maximum surface water lithium concentrations were measured (Figure 5), suggesting rapid chemical addition and removal of Li in the surface ocean, and a close relationship between the source and sink. The implication of the measured variability in lithium concentration within the upper water column in parts of the ocean, and lithium depletion in the deep waters of the North Pacific and North Atlantic Oceans (Figures 3 and 5; Angino & Billings, 1966; Fabricand et al., 1966; Stoffyn-Egli & Mackenzie, 1984), is that despite no significant known role for lithium in biological systems or in redox cycles, the oceanic lithium cycle is far more active than implied by its global-ocean residence time based on the riverine and hydrothermal input.
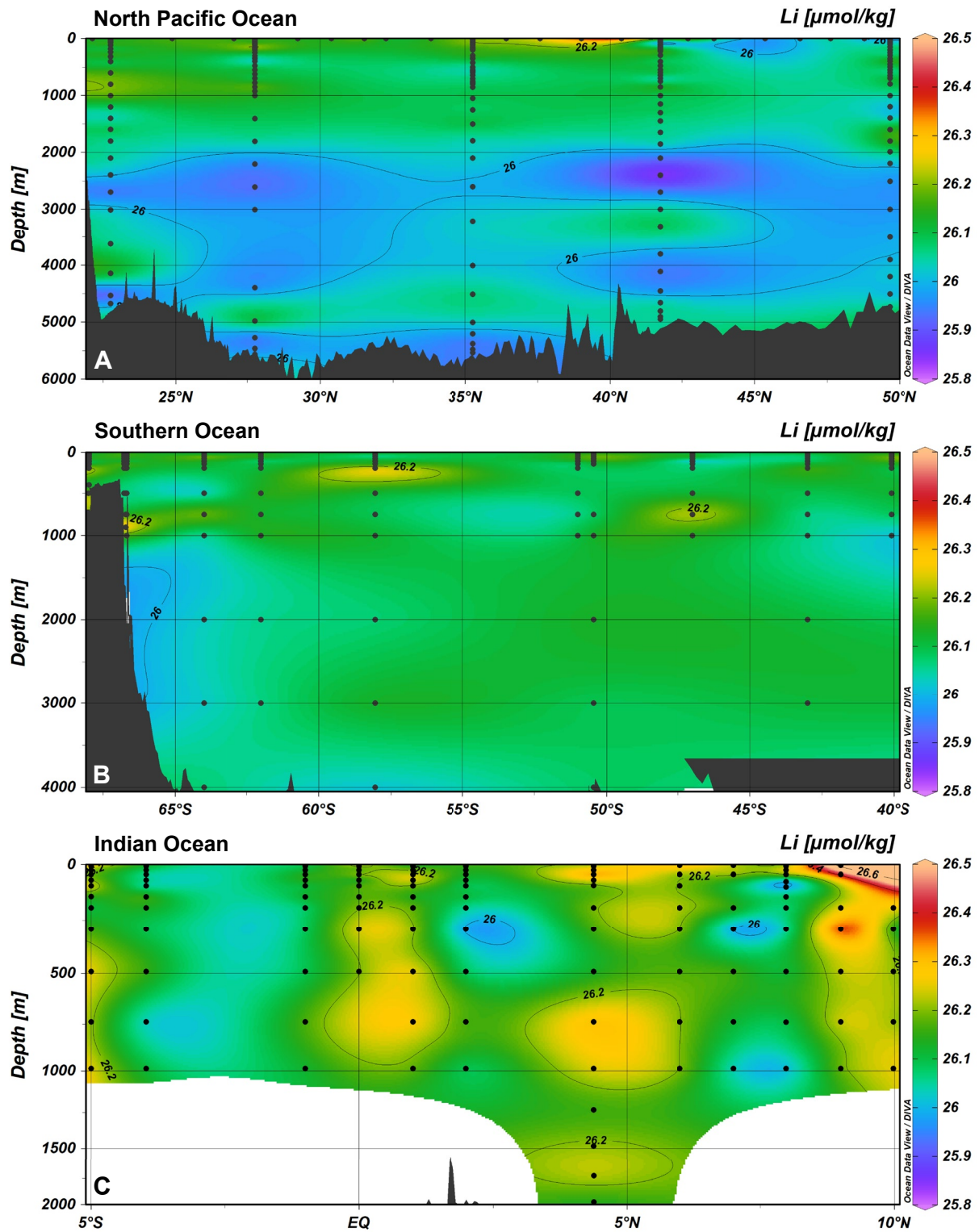
Figure 3. Dissolved salinity-normalized lithium concentrations in the North Pacific (a), Southern (b) and Indian (c) Ocean sections.
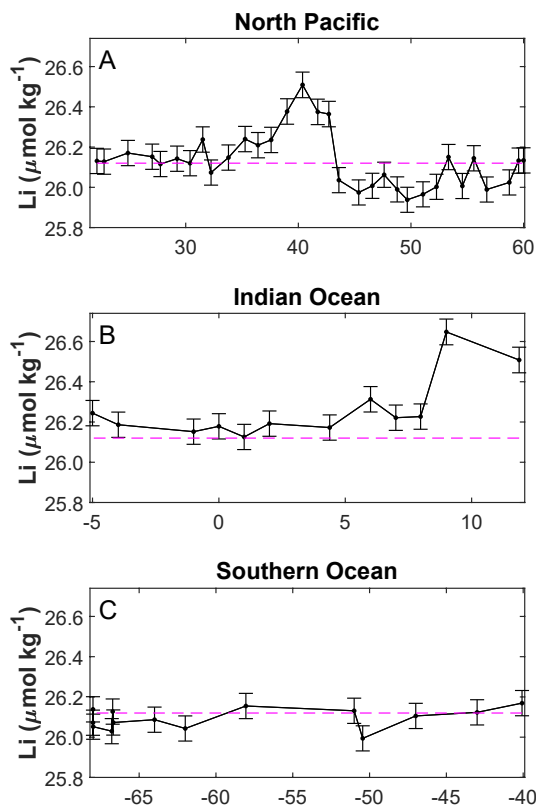
Figure 4. Salinity-normalized lithium concentrations in the surface water of the North Pacific, Indian Ocean and Southern Ocean sections. Surface is defined as the shallowest water sample collected from each station, typically within the top 5 m of the water column. The horizontal dashed line marks the mean lithium concentration of all samples analyzed in this study, from all oceans. Error bars are the long-term $\pm 2\sigma$ SD of repeat analyses of the consistency standard as additional samples (Figure 2).

4.1. Source of Surface Water Excess Lithium

Increased lithium concentrations in the surface waters of remote North Pacific and Indian Ocean locations imply that the source of the lithium is likely from atmospheric deposition (Figures 4–6). The likely sources of atmospheric deposition to the central North Pacific are dust and anthropogenic aerosols blown from east Asia (Uematsu et al., 1983). The increase in dissolved lithium concentrations in surface water that is observed in the northern Indian Ocean also suggests atmospheric deposition, as that region is also associated with elevated fluxes of both dust and anthropogenic aerosols (Aswini et al., 2020).

The maximum Li_{xs_tot} flux measured in the North Pacific section of CLIVAR P16 is 240 nmol $m^{-2}\,d^{-1}$ (Figure 6). A cubic meter of seawater at the surface of the ocean would typically contain 26.1 mmol of dissolved lithium, so it would require 300 years to generate a 2% increase in lithium concentrations of the top 50 m alone, if all lithium deposited by dust is released to the water. The circulation time of the entire Pacific Ocean is ~1,000 years (Matsumoto, 2007), therefore the aerosol lithium flux measured on the P16N cruise is too small to account for the observed surface seawater accumulation. However, aerosol lithium concentrations are higher in aerosols from the western part of the North Pacific (Figure S2 in Supporting Information S1), upstream of the Kuroshio extension and Oyashio currents that carry surface water to the study region. It is also likely that aerosol fluxes and their chemical composition vary greatly in time, hence the 24-hr collections conducted on a different season, 12 years before the CDisK-IV cruise, may not represent the same conditions as the seawater samples collected during that cruise.

Wind-blown dust can provide lithium to the surface ocean by several different mechanisms including congruent dissolution of dust particles (adding elements to seawater at the same proportions found in the dissolving solid), release of lithium adsorbed to the surface of clay minerals, and dissolution of secondary phases such as Fe-Mn oxides. We will now explore if dissolution of mineral dust could account for the measured North Pacific surface lithium enrichment. Loess from Chinese deserts has a likely composition of 40 ppm lithium and 13% Al_2O_3 (Teng et al., 2004), which translates to Li/Al = 0.0023 mol mol^{-1}. Buck et al. (2013) report maximum aerosol total aluminium fluxes of 8,500 nmol $m^{-2}\,d^{-1}$ in the subpolar-subtropical transition zone (and higher fluxes in the direction of the Asian continent), and it has been previously suggested that ~10% of the aluminium found in Asian dust dissolves in seawater (Maring & Duce, 1987). These numbers hint that dissolution of mineral dust may supply 2 nmol lithium $m^{-2}\,d^{-1}$. Although there is almost an order of magnitude uncertainty around this number, this does not change the conclusion that congruent dissolution of mineral dust is not the major source of lithium to the surface ocean. Note, however, that lithium is not evenly distributed among the main groups of minerals comprising the upper continental crust. Phyllosilicates are higher in lithium and have lower δ^7Li values than quartz and plagioclase, hence small particles that can travel long distances carry more lithium than large mineral particles (Garzanti et al., 2011; Sauzéat et al., 2015).

The distribution of lithium concentrations in the upper ocean, and the qualitative agreement between bulk aerosol deposition data and the water chemistry data, suggest that the excess lithium is aerosol derived. The North Pacific study region is remote; any lithium supplied by rivers or subterranean discharge should be well mixed in the water column and penetrate to deeper depths before reaching this transect. We shall use the lithium isotopes to consider these possibilities. The δ^7Li value of the upper continental crust is $0.6 \pm 0.6‰$ (Sauzéat et al., 2015; Teng et al., 2004), much lower than the δ^7Li value of seawater ($30.8 \pm 0.4‰$; Carignan et al., 2004; Rosner et al., 2007). Formation of authigenic clays involves lithium isotope fractionation with $\alpha = 0.99$, which means δ^7Li values of authigenic clays are 10‰ lower than the solution they precipitated from (Vigier et al., 2008). A simple two-endmember mass balance between seawater and dust suggests that a 2.5% enrichment of surface
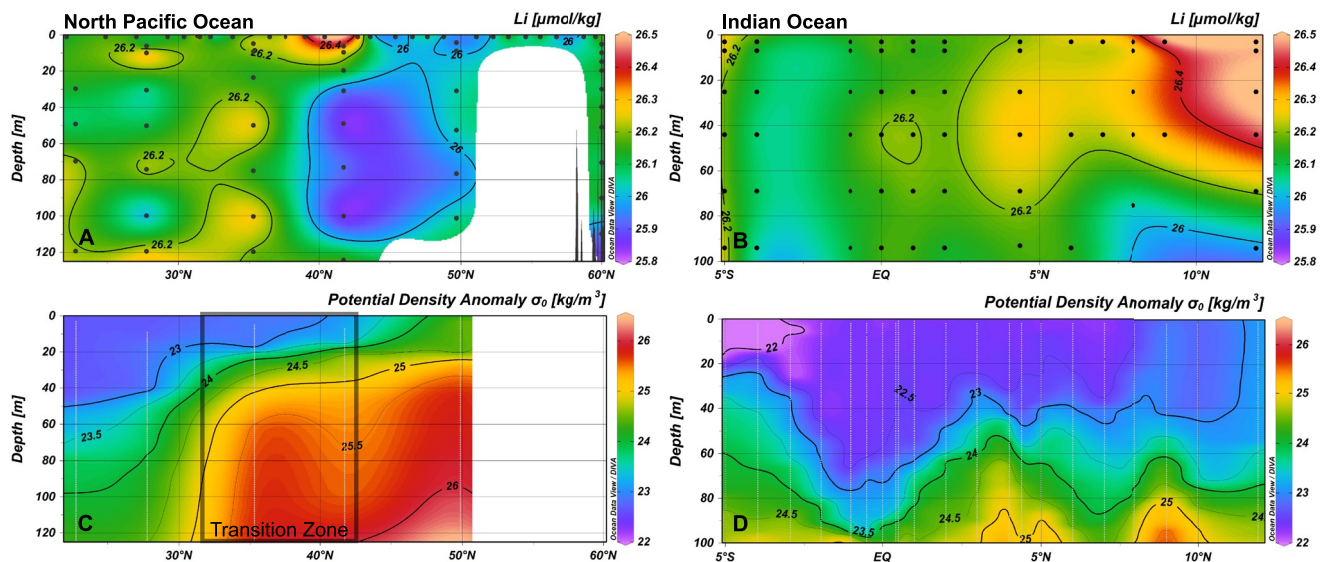
Figure 5. Dissolved salinity-normalized lithium concentrations in the upper water column of the (a) North Pacific and (b) tropical Indian Ocean sections. Panels (c, d) illustrate the potential density anomaly calculated using the CTD data from the CDisK-IV and SN105 cruises. The rectangle in panel (c) illustrates the boundaries of the transition zone between the subtropical and subpolar gyres of the North Pacific.

seawater lithium concentrations by congruent dissolution of dust would decrease δ^7Li values of the seawater by 0.8‰, though this could be counteracted if there is a lithium isotope fractionation on the formation of or adsorption of lithium on clay minerals. The analytical uncertainty of ∼0.4‰ makes it hard to detect a dust contribution of ≤50% if the other input has δ^7Li values similar to seawater. Absence of a dust derived δ^7Li signal is consistent with the calculation suggesting that dissolution of mineral dust is not the main source of dissolved lithium to the ocean. An alternative hypothesis is that much of the excess lithium sourced to the surface ocean is adsorbed onto wind-blown clays or manganese oxides, and is not within mineral crystals. Clay particles have high capacity for adsorption of lithium in freshwater but very low capacity for adsorption of lithium in seawater because lithium is outcompeted for adsorption sites by sodium (Hindshaw et al., 2019). Ion-exchange of lithium on clay minerals can therefore be a source of lithium to the surface ocean but are less likely to be a sink. Adsorption of lithium from water onto alteration minerals such as smectite or gibbsite involves relatively little isotope fractionation, hence desorption of this lithium cannot be detected in analyses of seawater δ^7Li values (Hindshaw et al., 2019; Pistiner & Henderson, 2003; Wimpenny et al., 2015).
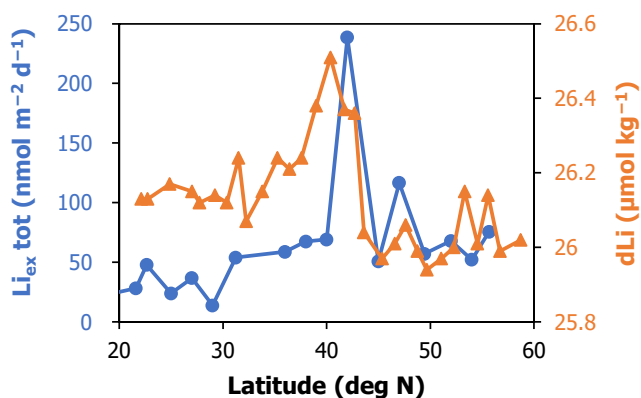

Figure 6. Comparison between aerosol total excess lithium flux, calculated by subtraction of sea-salt lithium using chlorine concentrations measured using XRF for samples collected during the CLIVAR P16 cruise (February to March 2006), and surface dissolved salinity normalized lithium concentrations analyzed on samples collected during cruise CDisK-IV (August 2017).

Shallow water in the northern part of the North Pacific subtropical gyre is low in dissolved aluminium but rich in dissolved lead (Figure 7; Zheng et al., 2019). This is somewhat inconsistent with the aerosol data (Figure 6) because the region that receives the highest aerosol aluminium fluxes has particularly low surface dissolved aluminium concentrations, and suggests that continental inputs from Hawaii and North America are sustained sources of aluminium, whereas aerosol supplied aluminium is quickly removed from the surface seawater. The surface water concentrations of lithium are therefore better correlated with an anthropogenic contaminant, lead, than with aluminium, a proxy of mineral dust. The lithium concentration peak is narrower than the dissolved lead concentration peak. This suggests that most of the excess lithium comes from a limited geographic region, unlike lead pollution that originates from multiple Asian countries. Schlesinger et al. (2021) calculated that coal combustion comprised 53% of the total atmospheric emission of lithium in 2019, without sea-spray. 33.1% of the global production of coal took place in the northern China provinces of Shanxi and Inner Mongolia, and this coal is 8 times higher in lithium than coal from the rest of the world, including other Chinese sources. This means that in 2019, approximately
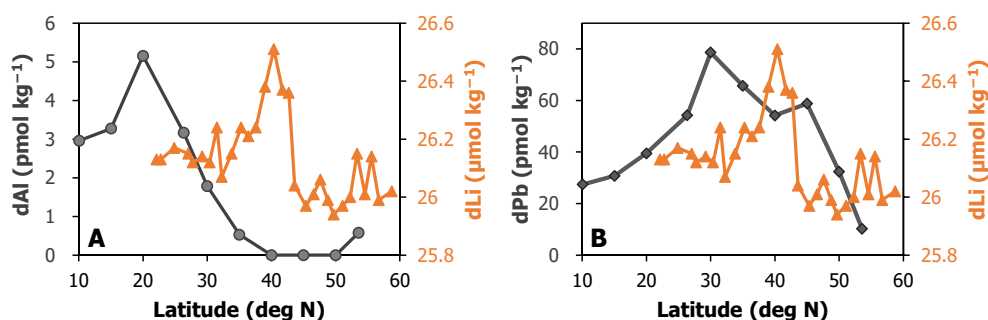
Figure 7. Comparison of North Pacific surface dissolved lithium data from cruise CDisK-IV (~150°W, August 2017) with surface dissolved aluminium (a) and surface dissolved lead (b) data from cruise KH-05-02 (160°W, August to September 2005; Zheng et al., 2019).

80% of the fly ash lithium emitted to the atmosphere originated in northern China. It seems that the narrow geographic provenance of high lithium coal coincides with the temporal variability in anthropogenic emissions of aerosol lithium and may produce the difference in shape between their surface water distributions. The production of Chinese coal tripled between 2000 and 2009, and continued to grow since (BP, 2021; Dai et al., 2011) while surface ocean lead concentrations have been roughly constant in the North Pacific since the mid 1970s (Zheng et al., 2019). High lead concentrations are found in the top 400 m of the water column (Zheng et al., 2019) whereas the data suggest excess lithium is removed within the top 100 m (Figure 5); these observations support the longer lasting supply and stability in the water column of anthropogenic lead in the North Pacific. Overall, these comparisons suggest that lithium and lead delivery to the ocean follow similar pathways, while the removal of lithium could be associated with removal of aluminium.

4.2. Removal of Lithium From Seawater

Ocean deep waters form in the high latitude North Atlantic and Southern Oceans, mix within the Southern Ocean, and flow northward from the Southern Ocean to fill the deep basins of the Pacific and Indian Oceans (Carter et al., 2008; Rae & Broecker, 2018). A slight decrease in seawater lithium concentrations by 0.11 ± 0.03 μmol kg^{-1} below 2,000 m in the North Pacific compared to the Southern Ocean end-members of AABW and Lower Circumpolar Deep Water (LCDW) suggests a deep-sea sink for lithium in the Pacific Ocean (Figure 3). Evidence for removal of lithium is found in the close association between the highest and lowest concentrations of lithium in shallow waters (see above), and there is no evidence for removal or supply of lithium in intermediate waters. We shall now discuss possible mechanisms for removal of lithium in the surface and deep ocean.

Methods used to harvest lithium from seawater for industrial applications have revealed that manganese and aluminium oxides can rapidly adsorb large amounts of lithium (Liu et al., 2015; Takeuchi, 1980; Wajima et al., 2012). Environmental studies support that manganese nodules and gibbsite react with lithium (Chan & Hein, 2007; Jiang et al., 2007; Pistiner & Henderson, 2003; Wimpenny et al., 2015). The final sink for most seawater lithium is in clay minerals, formed in the ocean during alteration of basalt or authigenically in marine sediments (Andrews et al., 2020; Li & West, 2014; Seyfried et al., 1984).

4.2.1. Removal From the Surface Ocean

In this section, we discuss the potential mechanisms that can lead to lithium removal from the surface ocean. Our discussion is based on the existing knowledge on aluminium and manganese cycling, used as analogs for possible processes removing lithium from the water column.

Leaching experiments in de-ionized water and filtered seawater of aerosols collected in the Pacific Ocean suggest release of 3.7% and 45% of the aerosol aluminium and manganese, respectively (Buck et al., 2013). Similar values were measured in the eastern Indian Ocean (Grand et al., 2015). Seawater-dissolved aluminium and manganese are in the low nM range in the North Pacific and tropical Indian Oceans, despite high fluxes derived from aerosol deposition, suggesting rapid removal of these elements from seawater, yet little aluminium and manganese is found in pure particulate and colloidal forms (Vu & Sohrin, 2013; Zheng et al., 2019). Aluminium is not bio-active yet its removal is far faster in the surface than deep ocean (Singh et al., 2020). Angel et al. (2016)

experimentally studied the solubility of aluminium hydroxides in seawater. They found that the solubility of aluminium hydroxides is much greater than the aluminium concentrations of any ocean waters. They also found that less than 40% of the aluminium is removed by adsorption, even in the presence of an extremely high load of suspended solids. According to these experiments, when the amount of aluminium added is higher than its solubility, an initial precipitate forms and induces precipitation of hydrotalcite ($Mg_6Al_2CO_3(OH)_{16} \cdot 4H_2O$) over the course of a few weeks. It is thus possible that similar reactions should be a sink for lithium.

In the open ocean, bulk aluminium concentrations are never high enough to induce this set of reactions but it is likely that dissolved aluminium concentrations are much higher at the micrometer range around recently deposited dust, and that these particles scavenge additional aluminium. The dust particles themselves can also act as nucleation sites for such reactions. An alternative location in the surface ocean where aluminium hydroxides might form is around photosynthesizing phytoplankton and cyanobacteria. Photosynthesizing cells consume CO_2 and locally increase the pH and, by extension, the concentration of carbonate ion (Gattuso et al., 1999). Biologically-induced mineralization by local alteration of seawater chemistry has been observed near various prokaryotes (Frankel & Bazylinski, 2003), and may be an important factor in the formation of aluminium hydroxides and hydrotalcite. Specific uptake of aluminium by diatoms was observed in the North Atlantic and in mesocosm experiments (Menzel Barraqueta et al., 2018; Moran & Moore, 1988). These mechanisms may explain why removal of aluminium and aerosol derived lithium is rapid in the photic zone.

Oxidation of manganese and removal of lithium through the formation of manganese oxides requires a simpler mechanism (Hein et al., 2020). Reduced manganese is rapidly oxidized through a variety of microbial reactions. These reactions transform the majority of the dissolved manganese into water insoluble MnO_2, which is removed from seawater by direct settling or via aggregation by particulate matter (van Hulten et al., 2017). The scale of this process is not sufficient to solely explain the concentration gradient we measured in the surface ocean because lithium is a minor constituent in manganese oxides.

4.2.2. Removal in the Deep Ocean

Adsorption onto manganese oxides is likely a sink for lithium in the surface ocean, and is a sink for lithium in the deep ocean, yet the magnitude of the sink of lithium into manganese nodules is small (Chan & Hein, 2007; Jiang et al., 2007). The Pacific sea floor is covered with large numbers of Fe-Mn nodules, but these nodules probably stay exposed at the surface for long periods of time (Cronan, 1977), and their adsorption capacity for lithium may be limited (Chan & Hein, 2007). We suggest that this may explain why most of the lithium remains in the water column and also hints at a sink-switch mechanism, in which adsorbed lithium desorbs from manganese nodules and enters newly-forming authigenic clay minerals.

The process of lithium incorporation in authigenic clay minerals was demonstrated in low-temperature hydrothermal weathering of basalt in the ocean (Seyfried et al., 1984; Zhang et al., 1998). Its importance in deep-sea sediments far from hydrothermal sites is not well constrained but was suggested to be a major component of the marine lithium cycle (Andrews et al., 2020; Stoffyn-Egli & Mackenzie, 1984). If we assume it takes AABW and LCDW 1,000 years to reach the North Pacific study sites (Matsumoto, 2007), that lithium concentrations decrease over this time by 0.11 ± 0.03 µmol kg^{-1} in the bottom 3,000 m of the water column (Figure 3), and that the lithium content of authigenic clay minerals is 300 ppm (Hein et al., 1979), then the average accumulation rate of authigenic clays would need to be 8 ± 3 kg m^{-2} ka^{-1}. Assuming average clay density of 2.7 g cm^{-3}, and bulk sediment porosity of 0.5, the basin-wide average authigenic clay accumulation rate would be 0.6 ± 0.2 cm ka^{-1}. Average bulk sediment accumulation rates in the North Pacific vary between 0.3 cm ka^{-1} in the subtropical gyre and 1.5 cm ka^{-1} in the subpolar gyre (Opdyke & Foster, 1970), and Hein et al. (1979) have previously shown that authigenic clay minerals account for 10% to >50% of the sediment in a manganese-nodule-rich area of the tropical North Pacific. This means that the rate of authigenic clay formation implied by the lithium depletion is high, but possible, considering that authigenic clay formation rates are much higher per unit area in deep-sea basalts (Seyfried et al., 1984; Zhang et al., 1998), and probably also in productive areas with higher fluxes of diatoms to the sediment (Ehlert et al., 2016) than in the low-productivity subtropical gyre. Several recent studies have suggested that authigenic precipitation of clay minerals is more common in the modern ocean than previously thought (Andrews et al., 2020; Baronas et al., 2017; Dunlea et al., 2017; Rahman, 2019) and our North Pacific lithium data appear consistent with this conclusion.

5. Implications

Overall, the observed lithium concentration spatial heterogeneity in the Southern and Pacific Oceans appears somewhat contradictory with the assumed long residence time of lithium in the ocean. Assuming lithium concentration of 26.11 μmol kg^{-1} in the Southern Ocean water masses, and a transit time of 1,000 years from the Southern Ocean to the North Pacific, the measured 0.11 ± 0.03 μmol kg^{-1} decrease in salinity normalized lithium concentration from the Southern Ocean to the deep North Pacific suggests that the current residence time of lithium with respect to removal in the deep ocean is less than or equal to $240,000 \pm 70,000$ years. This implies that the residence time of lithium in the ocean is much shorter than the 1.5–1.8 Ma calculated from the riverine flux of dissolved lithium (Huh et al., 1998; Lecuyer, 2016). This leads to the suggestion that there may be a large imbalance between the historically established sources and sinks for dissolved lithium. To match the deep ocean removal rate we suggest, there would need to be additional lithium sources that are 4–5 fold larger than the direct fluxes of dissolved lithium from rivers and hydrothermal vents.

We have to qualify that the calculation of residence time based on water column profiles of an element may be biased by processes that do not lead to permanent removal. This is the common case for nutrient type elements, for example, strontium concentrations vary by 2%–3% between surface and deep waters and between different ocean basins due to strontium uptake in the mineralization of $SrSO_4$ and $CaCO_3$ and release of strontium when these minerals dissolve at depth, even though the residence time of strontium in the ocean is 2–3 Ma (de Villiers, 1999; Steiner et al., 2020). The water column profiles of scavenged type elements, elements whose concentrations decrease with depth in the water column, generally reflect their residence time in the ocean because of limited regeneration and return flux from the sediment. Lithium is unique because the general decrease in lithium concentrations with depth suggest some scavenging behavior, but contrary to scavenged-type elements lithium is water soluble and not particularly particle reactive.

Porewater lithium profiles from ODP and IODP sites suggest that coastal and terrigenous sediments are generally a source for lithium, while open ocean sites are normally a sink (Andrews et al., 2020). Jeandel and Oelkers (2015) suggested that dissolution of terrigenous particulate material is a larger source of strontium, neodymium, silicon and iron to the ocean than riverine and hydrothermal transport of dissolved ions. The lithium concentration data are consistent with this hypothesis. It should therefore be considered if the water column lithium profiles reflect a transition between net dissolution of aluminosilicate minerals in coastal and shallow sediments, yielding a net sedimentary source of lithium, to increasing relative importance of clay authigenesis in deep-sea sediments, yielding a net sedimentary lithium sink (Andrews et al., 2020).

The global lithium cycle is currently strongly out of balance because anthropogenic activities have increased the mobilization of lithium by 500% (Schlesinger et al., 2021). The anthropogenic perturbation may explain the observed surface ocean patterns in lithium concentrations. What speaks against this notion is that most of the increase in lithium input due to anthropogenic activities took place in recent decades, which does not give enough time to transfer this signal to the deep waters of the Southern Ocean, particularly considering that atmospheric deposition in the Southern Ocean is low (Buck et al., 2013; Martin, 1990).

In summary, while recent increased anthropogenic mobilization of lithium could account for some of the changes in surface ocean concentrations we report, they cannot be responsible for the apparent high scavenging rate we see in the deep Pacific. Application of this high scavenging rate to the global deep ocean would lead to the unrealistic conclusion that there is a missing source for dissolved lithium that is 4–5 times greater than the known sources. A possible solution for this conundrum is that dissolution of terrigenous particulate material is a larger source of lithium to the ocean than transport of dissolved lithium by rivers.

Data Availability Statement

Data associated with this manuscript are available as supporting online information and in the Panaea data depository https://doi.pangaea.de/10.1594/PANGAEA.941888.

References

Andrews, E., Pogge von Strandmann, P. A. E., & Fantle, M. S. (2020). Exploring the importance of authigenic clay formation in the global Li cycle. *Geochimica et Cosmochimica Acta*, *289*, 47–68. https://doi.org/10.1016/j.gca.2020.08.018

Angel, B. M., Apte, S. C., Batley, G. E., & Golding, L. A. (2016). Geochemical controls on aluminium concentrations in coastal waters. *Environmental Chemistry*, *13*, 111–118. https://doi.org/10.1071/en15029

Angino, E. E., & Billings, G. K. (1966). Lithium content of sea water by atomic absorption spectrometry. *Geochimica et Cosmochimica Acta*, *30*, 153–158. https://doi.org/10.1016/0016-7037(66)90104-9

Aswini, A. R., Hegde, P., Aryasree, S., Girach, I. A., & Nair, P. R. (2020). Continental outflow of anthropogenic aerosols over Arabian Sea and Indian ocean during wintertime: ICARB-2018 campaign. *Science of The Total Environment*, *712*, 135214. https://doi.org/10.1016/j.scitotenv.2019.135214

Ayers, J. M., & Lozier, M. S. (2010). Physical controls on the seasonal migration of the North Pacific transition zone chlorophyll front. *Journal of Geophysical Research*, *115*, C05001. https://doi.org/10.1029/2009jc005596

Baker, A. R., Landing, W. M., Bucciarelli, E., Cheize, M., Fietz, S., Hayes, C. T., et al. (2016). Trace element and isotope deposition across the air–sea interface: Progress and research needs. *Philosophical Transactions of the Royal Society A: Mathematical, Physical & Engineering Sciences*, *374*, 20160190. https://doi.org/10.1098/rsta.2016.0190

Baronas, J. J., Hammond, D. E., McManus, J., Wheat, C. G., & Siebert, C. (2017). A global Ge isotope budget. *Geochimica et Cosmochimica Acta*, *203*, 265–283. https://doi.org/10.1016/j.gca.2017.01.008

Bohlin, M. S., & Bickle, M. J. (2019). The reactive transport of Li as a monitor of weathering processes in kinetically limited weathering regimes. *Earth and Planetary Science Letters*, *511*, 233–243. https://doi.org/10.1016/j.epsl.2019.01.034

Bohlin, M. S., Misra, S., Lloyd, N., Elderfield, H., & Bickle, M. J. (2018). High-precision determination of lithium and magnesium isotopes utilising single column separation and multi-collector inductively coupled plasma mass spectrometry. *Rapid Communications in Mass Spectrometry*, *32*, 93–104. https://doi.org/10.1002/rcm.8020

BP. (2021). Statistical review of world energy.

Brunskill, G. J., Zagorskis, I., & Pfitzner, J. (2003). Geochemical mass balance for lithium, boron, and strontium in the Gulf of Papua, Papua New Guinea (project TROPICS). *Geochimica et Cosmochimica Acta*, *67*, 3365–3383. https://doi.org/10.1016/s0016-7037(02)01410-2

Buck, C. S., Landing, W. M., & Resing, J. (2013). Pacific Ocean aerosols: Deposition and solubility of iron, aluminum, and other trace elements. *Marine Chemistry*, *157*, 117–130. https://doi.org/10.1016/j.marchem.2013.09.005

Carignan, J., Cardinal, D., Eisenhauer, A., Galy, A., Rehkamper, M., Wombacher, F., & Vigier, N. (2004). A reflection on Mg, Cd, Ca, Li and Si isotopic measurements and related reference materials. *Geostandards and Geoanalytical Research*, *28*, 139–148. https://doi.org/10.1111/j.1751-908x.2004.tb01050.x

Carignan, J., Vigier, N., & Millot, R. (2007). Three secondary reference materials for lithium isotope measurements: Li7-N, Li6-N and LiCl-N solutions. *Geostandards and Geoanalytical Research*, *31*, 7–12. https://doi.org/10.1111/j.1751-908x.2007.00833.x

Carter, L., McCave, I. N., & Williams, M. J. M. (2008). Circulation and water masses of the Southern Ocean: A review. In F. Florindo, & M. Siegert (Eds.), *Developments in Earth and environmental sciences* (pp. 85–114). Elsevier.

Chan, L.-H., & Edmond, J. M. (1988). Variation of lithium isotope composition in the marine environment: A preliminary report. *Geochimica et Cosmochimica Acta*, *52*, 1711–1717. https://doi.org/10.1016/0016-7037(88)90239-6

Chan, L.-H., & Hein, J. R. (2007). Lithium contents and isotopic compositions of ferromanganese deposits from the global ocean. *Deep Sea Research Part II: Topical Studies in Oceanography*, *54*, 1147–1162. https://doi.org/10.1016/j.dsr2.2007.04.003

Chow, T., & Goldberg, E. (1962). Mass spectrometric determination of lithium in seawater. *Journal of Marine Research*, *20*, 163–167.

Cronan, D. S. (1977). *Deep-sea nodules: Distribution and geochemistry*. In G. P. Glasby (Ed.), *Elsevier oceanography Series* (pp. 11–44). Elsevier.

Cummins, P. F., & Freeland, H. J. (2007). Variability of the north Pacific current and its bifurcation. *Progress in Oceanography*, *75*, 253–265. https://doi.org/10.1016/j.pocean.2007.08.006

Dai, S., Ren, D., Chou, C.-L., Finkelman, R., Seredin, V., & Zhou, Y. (2011). Geochemistry of trace elements in Chinese coals: A review of abundances, genetic types, impacts on human health, and industrial utilization. *International Journal of Coal Geology*, *94*, 3–21. https://doi.org/10.1016/j.coal.2011.02.003

Dellinger, M., West, A. J., Paris, G., Adkins, J. F., Pogge von Strandmann, P. A. E., Ullmann, C. V., et al. (2018). The Li isotope composition of marine biogenic carbonates: Patterns and mechanisms. *Geochimica et Cosmochimica Acta*, *236*, 315–335. https://doi.org/10.1016/j.gca.2018.03.014

deVilliers, S. (1999). Seawater strontium and Sr/Ca variability in the Atlantic and Pacific oceans. *Earth and Planetary Science Letters*, *171*, 623–634. https://doi.org/10.1016/s0012-821x(99)00174-0

deVilliers, S., Greaves, M., & Elderfield, H. (2002). An intensity ratio calibration method for the accurate determination of Mg/Ca and Sr/Ca of marine carbonates by ICP-AES. *Geochemistry, Geophysics, Geosystems*, *3*, 1001. https://doi.org/10.1029/2001gc000169

Dunlea, A. G., Murray, R. W., Ramos, D. P. S., & Higgins, J. A. (2017). Cenozoic global cooling and increased seawater Mg/Ca via reduced reverse weathering. *Nature Communications*, *8*, 844. https://doi.org/10.1038/s41467-017-00853-5

Edmond, J. M., Measures, C., McDuff, R. E., Chan, L. H., Collier, R., Grant, B., et al. (1979). Ridge crest hydrothermal activity and the balances of the major and minor elements in the ocean: The Galapagos data. *Earth and Planetary Science Letters*, *46*, 1–18. https://doi.org/10.1016/0012-821x(79)90061-x

Ehlert, C., Doering, K., Wallmann, K., Scholz, F., Sommer, S., Grasse, P., et al. (2016). Stable silicon isotope signatures of marine pore waters—Biogenic opal dissolution versus authigenic clay mineral formation. *Geochimica et Cosmochimica Acta*, *191*, 102–117. https://doi.org/10.1016/j.gca.2016.07.022

Fabricand, B. P., Imbimbo, E. S., Brey, M. E., & Weston, J. A. (1966). Atomic absorption analyses for Li, Mg, K, Rb, and Sr in ocean waters. *Journal of Geophysical Research*, *71*, 3917–3921. https://doi.org/10.1029/jz071i016p03917

Frankel, R. B., & Bazylinski, D. A. (2003). Biologically induced mineralization by bacteria. *Reviews in Mineralogy and Geochemistry*, *54*, 95–114. https://doi.org/10.2113/0540095

Fujinaga, T., Kuwamoto, T., Nakayama, E., & Tanaka, S. (1980). Determination of the lithium and rubidium in sea water by double channel flame emission spectrophotometry. *Journal of the Oceanographical Society of Japan*, *36*, 196–200. https://doi.org/10.1007/bf02070332

Garzanti, E., Andó, S., France-Lanord, C., Censi, P., Vignola, P., Galy, V., & Lupker, M. (2011). Mineralogical and chemical variability of fluvial sediments 2. Suspended-load silt (Ganga–Brahmaputra, Bangladesh). *Earth and Planetary Science Letters*, *302*, 107–120. https://doi.org/10.1016/j.epsl.2010.11.043

Gattuso, J.-P., Allemand, D., & Frankignoulle, M. (1999). Photosynthesis and calcification at cellular, organismal and community levels in coral reefs: A review on interactions and control by carbonate chemistry. *American Zoologist*, *39*, 160–183. https://doi.org/10.1093/icb/39.1.160

Ginoux, P., Chin, M., Tegen, I., Prospero, J. M., Holben, B., Dubovik, O., & Lin, S.-J. (2001). Sources and distributions of dust aerosols simulated with the GOCART model. *Journal of Geophysical Research*, *106*, 20255–20273. https://doi.org/10.1029/2000jd000053

Grand, M. M., Measures, C. I., Hatta, M., Hiscock, W. T., Buck, C. S., & Landing, W. M. (2015). Dust deposition in the eastern Indian Ocean: The ocean perspective from Antarctica to the Bay of Bengal. *Global Biogeochemical Cycles*, *29*, 357–374. https://doi.org/10.1002/2014gb004898

Hathorne, E. C., & James, R. H. (2006). Temporal record of lithium in seawater: A tracer for silicate weathering? *Earth and Planetary Science Letters*, *246*, 393–406. https://doi.org/10.1016/j.epsl.2006.04.020

Hein, J. R., Koschinsky, A., & Kuhn, T. (2020). Deep-ocean polymetallic nodules as a resource for critical materials. *Nature Reviews Earth & Environment*, *1*, 158–169. https://doi.org/10.1038/s43017-020-0027-0

Hein, J. R., Yeh, H.-W., & Alexander, E. (1979). Origin of iron-rich montmorillonite from the manganese nodule belt of the North Equatorial Pacific. *Clays and Clay Minerals*, *27*, 185–194. https://doi.org/10.1346/ccmn.1979.0270303

Hindshaw, R. S., Tosca, R., Goût, T. L., Farnan, I., Tosca, N. J., & Tipper, E. T. (2019). Experimental constraints on Li isotope fractionation during clay formation. *Geochimica et Cosmochimica Acta*, *250*, 219–237. https://doi.org/10.1016/j.gca.2019.02.015

Hood, R. R., Beckley, L. E., & Wiggert, J. D. (2017). Biogeochemical and ecological impacts of boundary currents in the Indian Ocean. *Progress in Oceanography*, *156*, 290–325. https://doi.org/10.1016/j.pocean.2017.04.011

Hou, Y., Hammond, D. E., Berelson, W. M., Kemnitz, N., Adkins, J. F., & Lunstrum, A. (2019). Spatial patterns of benthic silica flux in the North Pacific reflect upper ocean production. *Deep Sea Research Part I: Oceanographic Research Papers*, *148*, 25–33. https://doi.org/10.1016/j.dsr.2019.04.013

Huh, Y., Chan, L.-H., Zhang, L., & Edmond, J. M. (1998). Lithium and its isotopes in major world rivers: Implications for weathering and the oceanic budget. *Geochimica et Cosmochimica Acta*, *62*, 2039–2051. https://doi.org/10.1016/s0016-7037(98)00126-4

IOC., SCOR, & IAPSO. (2010). The international thermodynamic equation of seawater—2010: Calculation and use of thermodynamic properties, Intergovernmental Oceanographic Commission, Manuals and Guides No. 56 (p. 196). Retrieved from www.TEOS-10.org

Jeandel, C., & Oelkers, E. H. (2015). The influence of terrigenous particulate material dissolution on ocean chemistry and global element cycles. *Chemical Geology*, *395*, 50–66. https://doi.org/10.1016/j.chemgeo.2014.12.001

Jiang, X., Lin, X., Yao, D., Zhai, S., & Guo, W. (2007). Geochemistry of lithium in marine ferromanganese oxide deposits. *Deep Sea Research Part I: Oceanographic Research Papers*, *54*, 85–98. https://doi.org/10.1016/j.dsr.2006.10.004

Jickells, T. D., An, Z. S., Andersen, K. K., Baker, A. R., Bergametti, G., Brooks, N., et al. (2005). Global iron connections between desert dust, ocean biogeochemistry, and climate. *Science*, *308*, 67–71. https://doi.org/10.1126/science.1105959

Kadko, D., Landing, W. M., & Buck, C. S. (2020). Quantifying atmospheric trace element deposition over the ocean on a global scale with satellite rainfall products. *Geophysical Research Letters*, *47*, e2019GL086357. https://doi.org/10.1029/2019gl086357

Langer, G., Sadekov, A., Greaves, M., Nehrke, G., Probert, I., Misra, S., & Thoms, S. (2020). Li partitioning into coccoliths of Emiliania huxleyi: Evaluating the general role of "vital effects" in explaining element partitioning in biogenic carbonates. *Geochemistry, Geophysics, Geosystems*, *21*, e2020GC009129. https://doi.org/10.1029/2020gc009129

Lecuyer, C. (2016). Seawater residence times of some elements of geochemical interest and the salinity of the oceans. *Bulletin de la Societe Geologique de France*, *187*, 245–259. https://doi.org/10.2113/gssgfbull.187.6.245

Lemarchand, E., Chabaux, F., Vigier, N., Millot, R., & Pierret, M.-C. (2010). Lithium isotope systematics in a forested granitic catchment (Strengbach, Vosges Mountains, France). *Geochimica et Cosmochimica Acta*, *74*, 4612–4628. https://doi.org/10.1016/j.gca.2010.04.057

Li, G. J., & West, A. J. (2014). Evolution of Cenozoic seawater lithium isotopes: Coupling of global denudation regime and shifting seawater sinks. *Earth and Planetary Science Letters*, *401*, 284–293. https://doi.org/10.1016/j.epsl.2014.06.011

Liu, L., Zhang, H., Zhang, Y., Cao, D., & Zhao, X. (2015). Lithium extraction from seawater by manganese oxide ion sieve $MnO_2 \cdot 0.5H_2O$. *Colloids and Surfaces A: Physicochemical and Engineering Aspects*, *468*, 280–284. https://doi.org/10.1016/j.colsurfa.2014.12.025

Maring, H. B., & Duce, R. A. (1987). The impact of atmospheric aerosols on trace metal chemistry in open ocean surface seawater, 1. Aluminum. *Earth and Planetary Science Letters*, *84*, 381–392. https://doi.org/10.1016/0012-821x(87)90003-3

Martin, J. B., Kastner, M., & Elderfield, H. (1991). Lithium: Sources in pore fluids of Peru slope sediments and implications for oceanic fluxes. *Marine Geology*, *102*, 281–292. https://doi.org/10.1016/0025-3227(91)90012-s

Martin, J. H. (1990). Glacial-interglacial CO_2 change: The iron hypothesis. *Paleoceanography*, *5*, 1–13. https://doi.org/10.1029/pa005i001p00001

Matsumoto, K. (2007). Radiocarbon-based circulation age of the world oceans. *Journal of Geophysical Research*, *112*, C09004. https://doi.org/10.1029/2007jc004095

McDougall, T. J., & Barker, P. M. (2011). *Getting started with TEOS-10 and the Gibbs Seawater (GSW) Oceanographic Toolbox* (p. 28). SCOR/IAPSO WG127.

Menzel Barraqueta, J. L., Klar, J., Gledhill, M., Schlosser, C., Shelley, R., Planquette, H. F., et al. (2019). Atmospheric deposition fluxes over the Atlantic Ocean: A GEOTRACES case study. *Biogeosciences*, *16*, 1525–1542. https://doi.org/10.5194/bg-16-1525-2019

Menzel Barraqueta, J. L., Schlosser, C., Planquette, H., Gourain, A., Cheize, M., Boutorh, J., et al. (2018). Aluminium in the North Atlantic Ocean and the Labrador Sea (GEOTRACES GA01 section): Roles of continental inputs and biogenic particle removal. *Biogeosciences*, *15*, 5271–5286. https://doi.org/10.5194/bg-15-5271-2018

Millero, F. J., Feistel, R., Wright, D. G., & McDougall, T. J. (2008). The composition of standard seawater and the definition of the reference-composition salinity scale. *Deep Sea Research Part I: Oceanographic Research Papers*, *55*, 50–72. https://doi.org/10.1016/j.dsr.2007.10.001

Misra, S., & Froelich, P. N. (2012). Lithium isotope history of Cenozoic seawater: Changes in silicate weathering and reverse weathering. *Science*, *335*, 818–823. https://doi.org/10.1126/science.1214697

Moran, S. B., & Moore, R. M. (1988). Evidence from mesocosm studies for biological removal of dissolved aluminium from sea water. *Nature*, *335*, 706–708. https://doi.org/10.1038/335706a0

Opdyke, N. D., & Foster, J. H. (1970). Paleomagnetism of cores from the North Pacific. In J. D. Hays (Ed.), *Geological investigations of the North Pacific* (p. 323). Geological Society of America.

Pistiner, J. S., & Henderson, G. M. (2003). Lithium-isotope fractionation during continental weathering processes. *Earth and Planetary Science Letters*, *214*, 327–339. https://doi.org/10.1016/s0012-821x(03)00348-0

Pogge von Strandmann, P. A. E., James, R. H., van Calsteren, P., Gíslason, S. R., & Burton, K. W. (2008). Lithium, magnesium and uranium isotope behaviour in the estuarine environment of basaltic islands. *Earth and Planetary Science Letters*, *274*, 462–471. https://doi.org/10.1016/j.epsl.2008.07.041

Pogge von Strandmann, P. A. E., Opfergelt, S., Lai, Y.-J., Sigfússon, B., Gislason, S. R., & Burton, K. W. (2012). Lithium, magnesium and silicon isotope behaviour accompanying weathering in a basaltic soil and pore water profile in Iceland. *Earth and Planetary Science Letters*, *339–340*, 11–23. https://doi.org/10.1016/j.epsl.2012.05.035

Polovina, J. J., Howell, E. A., Kobayashi, D. R., & Seki, M. P. (2017). The transition zone chlorophyll front updated: Advances from a decade of research. *Progress in Oceanography*, *150*, 79–85. https://doi.org/10.1016/j.pocean.2015.01.006

Rae, J. W. B., & Broecker, W. (2018). What fraction of the Pacific and Indian oceans' deep water is formed in the Southern Ocean? *Biogeosciences*, *15*, 3779–3794. https://doi.org/10.5194/bg-15-3779-2018

Rahman, S. (2019). Reverse weathering reactions in marine sediments. In J. K. Cochran, H. J. Bokuniewicz, & P. L. Yager (Eds.), *Encyclopedia of ocean sciences* (3rd ed., pp. 216–227). Academic Press.

Riley, J. P., & Tongudai, M. (1964). The lithium content of sea water. *Deep-Sea Research and Oceanographic Abstracts*, *11*, 563–568. https://doi.org/10.1016/0011-7471(64)90002-6

Rochford, D. J. (1964). Salinity maxima in the upper 1000 metres of the north Indian ocean. *Marine and Freshwater Research*, *15*, 1–24. https://doi.org/10.1071/mf9640001

Roden, G. I. (1991). Subarctic-subtropical transition zone of the North Pacific: Large-scale aspects and mesoscale structure. In J. A. Wetherall (Ed.), *Biology, oceanography, and Fisheries of the North Pacific transition zone and Subarctic frontal zone Honolulu* (pp. 1–38).

Rosner, M., Ball, L., Peucker-Ehrenbrink, B., Blusztajn, J., Bach, W., & Erzinger, J. (2007). A simplified, accurate and fast method for lithium isotope analysis of rocks and fluids, and δ7Li values of seawater and rock reference materials. *Geostandards and Geoanalytical Research*, *31*, 77–88. https://doi.org/10.1111/j.1751-908x.2007.00843.x

Sauzéat, L., Rudnick, R. L., Chauvel, C., Garçon, M., & Tang, M. (2015). New perspectives on the Li isotopic composition of the upper continental crust and its weathering signature. *Earth and Planetary Science Letters*, *428*, 181–192. https://doi.org/10.1016/j.epsl.2015.07.032

Schlesinger, W. H., Klein, E. M., Wang, Z., & Vengosh, A. (2021). Global biogeochemical cycle of lithium. *Global Biogeochemical Cycles*, *35*, e2021GB006999. https://doi.org/10.1029/2021gb006999

Schlitzer, R. (2020). Ocean data View.

Schlosser, C., Schmidt, K., Aquilina, A., Homoky, W. B., Castrillejo, M., Mills, R. A., et al. (2018). Mechanisms of dissolved and labile particulate iron supply to shelf waters and phytoplankton blooms off South Georgia. *Southern Ocean. Biogeosciences*, *15*, 4973–4993. https://doi.org/10.5194/bg-15-4973-2018

Schmitt, A.-D., Vigier, N., Lemarchand, D., Millot, R., Stille, P., & Chabaux, F. (2012). Processes controlling the stable isotope compositions of Li, B, Mg and Ca in plants, soils and waters: A review. *Comptes Rendus Geoscience*, *344*, 704–722. https://doi.org/10.1016/j.crte.2012.10.002

Schrag, D. P. (1999). Rapid analysis of high-precision Sr/Ca ratios in corals and other marine carbonates. *Paleoceanography*, *14*, 97–102. https://doi.org/10.1029/1998pa900025

Seyfried, W. E., Janecky, D. R., & Mottl, M. J. (1984). Alteration of the oceanic crust: Implications for geochemical cycles of lithium and boron. *Geochimica et Cosmochimica Acta*, *48*, 557–569. https://doi.org/10.1016/0016-7037(84)90284-9

Shenoi, S. S. C., Shetye, S. R., Gouveia, A. D., & Michael, G. S. (1993). Salinity extrema in the Arabian Sea. *Mitteilungen aus dem Geologisch-Paläontologischen Institut der Universität Hamburg*, *76*, 37–49.

Singh, N. D., Chinni, V., & Singh, S. K. (2020). Dissolved aluminium cycling in the northern, equatorial and subtropical gyre region of the Indian Ocean. *Geochimica et Cosmochimica Acta*, *268*, 160–185. https://doi.org/10.1016/j.gca.2019.09.028

Steiner, Z., Sarkar, A., Prakash, S., Vinayachandran, P. N., & Turchyn, A. V. (2020). Dissolved strontium, Sr/Ca ratios, and the abundance of Acantharia in the Indian and Southern Oceans. *ACS Earth Space Chem*, *4*, 802–811. https://doi.org/10.1021/acsearthspacechem.9b00281

Steiner, Z., Turchyn, A. V., Harpaz, E., & Silverman, J. (2018). Water chemistry reveals a significant decline in coral calcification rates in the southern Red Sea. *Nature Communications*, *9*, 3615. https://doi.org/10.1038/s41467-018-06030-6

Stoffyn-Egli, P. (1982). Conservative behaviour of dissolved lithium in estuarine waters. *Estuarine, Coastal and Shelf Science*, *14*, 577–587. https://doi.org/10.1016/s0302-3524(82)80079-0

Stoffyn-Egli, P., & Mackenzie, F. T. (1984). Mass balance of dissolved lithium in the oceans. *Geochimica et Cosmochimica Acta*, *48*, 859–872. https://doi.org/10.1016/0016-7037(84)90107-8

Swain, B. (2017). Recovery and recycling of lithium: A review. *Separation and Purification Technology*, *172*, 388–403. https://doi.org/10.1016/j.seppur.2016.08.031

Takeuchi, T. (1980). Extraction of lithium from sea water with metallic aluminum. *Journal of Nuclear Science and Technology*, *17*, 922–928. https://doi.org/10.1080/18811248.1980.9732675

Teng, F. Z., McDonough, W. F., Rudnick, R. L., Dalpé, C., Tomascak, P. B., Chappell, B. W., & Gao, S. (2004). Lithium isotopic composition and concentration of the upper continental crust. *Geochimica et Cosmochimica Acta*, *68*, 4167–4178. https://doi.org/10.1016/j.gca.2004.03.031

Thibon, F., Weppe, L., Vigier, N., Churlaud, C., Lacoue-Labarthe, T., Metian, M., et al. (2021). Large-scale survey of lithium concentrations in marine organisms. *Science of The Total Environment*, *751*, 141453. https://doi.org/10.1016/j.scitotenv.2020.141453

Tomascak, P. B., Magna, T., & Dohmen, R. (2016). The surficial realm: Low temperature geochemistry of lithium. In P. B. Tomascak, T. Magna, & R. Dohmen (Eds.), *Advances in lithium isotope geochemistry* (pp. 157–189). Springer International Publishing.

Uematsu, M., Duce, R. A., Prospero, J. M., Chen, L., Merrill, J. T., & McDonald, R. L. (1983). Transport of mineral aerosol from Asia over the North Pacific Ocean. *Journal of Geophysical Research*, *88*, 5343–5352. https://doi.org/10.1029/jc088ic09p05343

van Hulten, M., Middag, R., Dutay, J. C., de Baar, H., Roy-Barman, M., Gehlen, M., et al. (2017). Manganese in the west Atlantic Ocean in the context of the first global ocean circulation model of manganese. *Biogeosciences*, *14*, 1123–1152. https://doi.org/10.5194/bg-14-1123-2017

Vigier, N., Decarreau, A., Millot, R., Carignan, J., Petit, S., & France-Lanord, C. (2008). Quantifying Li isotope fractionation during smectite formation and implications for the Li cycle. *Geochimica et Cosmochimica Acta*, *72*, 780–792. https://doi.org/10.1016/j.gca.2007.11.011

Vu, H. T. D., & Sohrin, Y. (2013). Diverse stoichiometry of dissolved trace metals in the Indian Ocean. *Scientific Reports*, *3*, 1745. https://doi.org/10.1038/srep01745

Wajima, T., Munakata, K., & Uda, T. (2012). Adsorption behavior of lithium from seawater using manganese oxide adsorbent. *Plasma and Fusion Research*, *7*, 2405021. https://doi.org/10.1585/pfr.7.2405021

Wimpenny, J., Colla, C. A., Yu, P., Yin, Q.-Z., Rustad, J. R., & Casey, W. H. (2015). Lithium isotope fractionation during uptake by gibbsite. *Geochimica et Cosmochimica Acta*, *168*, 133–150. https://doi.org/10.1016/j.gca.2015.07.011

Wyatt, N. J., Milne, A., Woodward, E. M. S., Rees, A. P., Browning, T. J., Bouman, H. A., et al. (2014). Biogeochemical cycling of dissolved zinc along the GEOTRACES South Atlantic transect GA10 at 40°S. *Global Biogeochemical Cycles*, *28*, 44–56. https://doi.org/10.1002/2013gb004637

Zender, C. S., Bian, H., & Newman, D. (2003). Mineral dust Entrainment and deposition (DEAD) model: Description and 1990s dust climatology. *Journal of Geophysical Research*, *108*, 4416. https://doi.org/10.1029/2002jd002775

Zhang, L., Chan, L.-H., & Gieskes, J. M. (1998). Lithium isotope geochemistry of pore waters from ocean drilling program Sites 918 and 919, Irminger Basin. *Geochimica et Cosmochimica Acta*, *62*, 2437–2450. https://doi.org/10.1016/s0016-7037(98)00178-1

Zheng, L., Minami, T., Konagaya, W., Chan, C.-Y., Tsujisaka, M., Takano, S., et al. (2019). Distinct basin-scale-distributions of aluminum, manganese, cobalt, and lead in the North Pacific Ocean. *Geochimica et Cosmochimica Acta*, *254*, 102–121. https://doi.org/10.1016/j.gca.2019.03.038